GA-Based Off-Line Parameter Estimation of the Induction Motor Model Including Magnetic Saturation and Iron Losses

ANGELO ACCETTA [ID][1] **(Member, IEEE), FRANCESCO ALONGE**[2] **(Senior Member, IEEE), MAURIZIO CIRRINCIONE**[3] **(Senior Member, IEEE), FILIPPO D'IPPOLITO** [ID][2] **(Member, IEEE), MARCELLO PUCCI**[1] **(Senior Member, IEEE), AND ANTONINO SFERLAZZA** [ID][2] **(Member, IEEE)**

(Invited Paper)

[1] Institute for Marine engineering (INM), Section of Palermo, National Research Council of Italy (CNR), 90146 Palermo, Italy
[2] Department of Engineering, University of Palermo, 90128 Palermo, Italy
[3] School of Engineering and Physics, University of the South Pacific, Laucala Campus, 0679 Suva, Fiji

CORRESPONDING AUTHOR: ANTONINO SFERLAZZA (e-mail: antonino.sferlazza@unipa.it)

ABSTRACT This paper, starting from recent papers in the scientific literature dealing with Rotating Induction Motor (RIM) dynamic modelling, as a first step, improves its space-vector dynamic model, including both the magnetic saturation and iron losses; The main original aspects of the proposed model are the following: 1) the magnetic saturation of the iron core has been described on the basis of both current versus flux and flux versus current functions, 3) it includes the iron losses, separating them in hysteresis and eddy current ones, 4) it includes the effect of the load on the magnetic saturation. Afterwards, it proposes an off-line technique for the estimation of electrical parameters of this model, which is based on Genetic Algorithms (GA). The proposed method is based on input-output measurements and needs neither the machine design geometrical data nor a Finite Element Analysis (FEA) of the machine. It focuses on the application of an algorithm based on the minimization of a suitable cost function depending on the stator current error. The proposed electrical parameters estimation method has been initially tested in numerical simulation and further verified experimentally on a suitably developed test set-up.

INDEX TERMS Identification, iron losses, magnetic saturation, parameter estimation, rotating induction motor (rim), space-vector dynamic model.

NOMENCLATURE

$\boldsymbol{u}_s = u_{sD} + j u_{sQ},$ $\boldsymbol{u}'_r = u_{rd} + j u_{rq}:$	space-vectors of the stator and rotor voltages in the stator reference frame
$\boldsymbol{i}_s = i_{sD} + j i_{sQ},$ $\boldsymbol{i}'_r = i_{rd} + j i_{rq}:$	space-vectors of the stator and rotor currents in the stator reference frame
$\boldsymbol{u}_s^{\psi_r} = u_{sx} + j u_{sy}$	space-vectors of the stator and rotor voltages
$\boldsymbol{u}'^{\psi_r}_r = u_{rx} + j u_{ry}:$	in the rotor-flux oriented reference frame
$\boldsymbol{i}_s^{\psi_r} = i_{sx} + j i_{sy},$	space-vectors of the stator and rotor currents

$\boldsymbol{i}'^{\psi_r}_r = i_{rx} + j i_{ry}:$	in the rotor-flux oriented reference frame
$\boldsymbol{\psi}_s = \psi_{sD} + j \psi_{sQ},$ $\boldsymbol{\psi}'_r = \psi_{rd} + j \psi_{rq},$ $\boldsymbol{\psi}_m = \psi_{md} + j \psi_{mq}$	space-vectors of the stator, rotor and magnetizing flux linkages in the stator reference frame
$\boldsymbol{\psi}_s^{\psi_r} = \psi_{sx} + j \psi_{sy},$ $\boldsymbol{\psi}'^{\psi_r}_r = \psi_{rx} + j \psi_{ry},$ $\boldsymbol{\psi}_m^{\psi_r} = \psi_{mx} + j \psi_{my}:$	space-vectors of the stator, rotor and magnetizing flux linkages in the rotor-flux oriented reference frame
L_s, L_r	stator, rotor and three-phase

L_m: magnetizing inductances
L_{σ_s} stator, rotor
L_{σ_r}:   leakage inductances
R_s, R_r stator, rotor and
R_m: iron losses resistances
t_e: electromagnetic torque
ω_r: rotor speed in electrical angles
ω_{mr}:   rotor flux speed in electrical angles.

I. INTRODUCTION

Scientific literature about either on-line or off-line estimation of Rotating Induction Machine (RIM) electrical parameters is huge [2]. A correct knowledge of the electrical parameters of the RIM is particularly important when high performance control, non-linear control or sensorless control of rotating induction machines is required, since their behaviour is highly dependent on the accurate knowledge of their parameters. This is, e.g., true in particular in applications in which the electrical drive works in field weakening, like in fly-wheel. The adopted methodologies range from traditional no-load and locked rotor tests to more sophisticated dynamical tests. In general, the problem has been faced up with two approaches. The first is based on the direct computation of some electrical parameters with the help of input voltage and current measurements (signal injection, spectral analysis, linear or non-linear regression). The second is based on the development of suitable observers (full-order or reduced-order observers, extended Kalman filter, model reference adaptive systems) of the state-variables of the machine (stator currents, flux linkages and, possibly, also the speed) where the accuracy of the state reconstruction depends on an adaptive estimation of some electrical parameters [3]–[7]. All the above cited parameter estimation methods are based on the classic space-vector dynamic model of the RIM which, however, neglects several important aspects of the machine behaviour, in particular the magnetic saturation of the iron core and the iron losses. The scientific literature, however, offers nowadays more accurate space-vector dynamic models able to consider many of these aspects. The approaches for dealing with the strong non-linearities arising from the adoption of ferromagnetic material in the core are significantly different [8]–[11]. A very interesting set of recent papers about induction machine modelling which include magnetic saturation and iron losses together with their corresponding identification techniques is the following [12]–[18]. The set of all these papers treat the magnetic saturation of the iron core on the basis of a current versus flux approach, since it more easily faceable up to with analytical expressions. In details, the inductance versus flux expressions are defined in order to fulfill the reciprocity conditions. Such expressions are derived so to take into consideration also the effect of the load torque on the magnetic saturation. To this aim, [15], after defining all the inductance terms including magnetic saturation, applies a simplification from the T to Γ circuit scheme with a resulting reduction of the order of the model, as well as of parameters describing the model itself. As a consequence, the dependence of the saturation on the load is

straightforward attributed to the global leakage flux (the stator and rotor currents coincide).

Starting from the set of papers [12]–[18], this paper initially improves the space-vector dynamic model by including both the magnetic saturation and iron losses as for the following aspects:

- The adopted model is based on the complete T space-vector electrical scheme of the RIM, implying an increase of the number of state variables and related parameters.
- The magnetic saturation of the iron core has been described on the basis of both current versus flux and flux versus current functions. Both formulations properly fulfill the reciprocity conditions. Correspondingly, both inductance versus flux and inductance versus current expressions have been deduced.
- The model includes the iron losses, by means of a time varying resistance, accounting separately the hysteresis and the eddy current losses.
- The model includes the effects of the load on the saturation, accounting individually the effects of the rotor and the stator. It is needed because of the assumption of validity of the T circuital scheme.

Afterwards, this paper focuses an off-line technique for the estimation of the electrical parameters of the above mentioned model by using genetic algorithms (GA) [19]. The proposed method belongs to the category of off-line methods based on input-output measurements and needs neither the machine design geometrical data nor a Finite Element Analysis (FEA) of the machine. The paper can be used as a first step for a RIM drive self-commissioning phase. It focuses on the application of an algorithm based on the minimization of a suitable cost function depending on the stator current error. The proposed electrical parameters estimation method has been initially tested in numerical simulation and further verified experimentally on a suitably set up test set-up.

A. COMPARISON WITH THE SCIENTIFIC LITERATURE

Very few papers in the scientific literature treat the identification of the parameters defining the dynamic model of the RIM, accounting for both the magnetic saturation of the iron core and the iron losses. The unique papers with which the proposed one could be compared are [15], [17] and [18]. In [17], the magnetic saturation of the stator inductance has been modelled with a current versus flux approach by a power function. Adaptation laws for the parameters of the function have been proposed based on the back EMF error. The magnetizing curve has been obtained applying two flux levels (one just below the saturation point and one close to the rated flux). No additional data fitting method is necessary as the power function parameters can be directly identified.. The leakage inductance has been identified by signal injection prior to the identification of the stator inductance. The parameters defining the cross saturation effects have not been estimated. In [18] the total leakage inductance has been obtained in different operating points by analyzing the response to

high-frequency voltage injection. Both the saturation-induced saliency and the influence of load variations are considered in the identification. Based on the identified total leakage inductance, an estimate of the stator inductance is obtained. In [15] it is explicitly claimed that the parameters of the model related to the cross-saturation have a limited influence on the saturation of the machine and that their estimation highly complicates the identification process. For this reason, in [15] such parameters have been assumed a priori known and foxed. Papers [15], [17] and [18] however are based on the inverse Γ model, whereas the proposed identification techniques is applied to the T model, implying that the separate effects of the stator and rotor leakage fluxes on the saturation are accounted for. Neither [15], [17] nor [18] explicitly estimate the parameters of the saturation model related to the cross saturation, whereas the proposed technique is able to estimate such parameters, even if with few simplifying assumptions. Both [15], [17] and [18] estimate the parameters with more than one test, while the proposed identification technique permits all the parameters of the model to be estimated with only one dynamic test. This important result has been obtained by selecting suitable speed and load profiles, which are sufficiently informative in order all the parameters to be estimated. The methods in [15], [17], [18] have been applied to identify only the parameters of the saturation model based on the current versus flux approach. On the contrary, the proposed identification method has been successfully applied both to the current versus flux and flux versus current approaches.

II. RIM SPACE-VECTOR DYNAMIC MONEL INCLUDING MAGNETIC SATURATION AND IRON LOSSES

The classic space-vector dynamic model of the RIM neglects the iron losses [20]. Such a simplifying assumption reflects strongly on the state formulation. As a matter of fact, even if the space-vector circuital scheme presents 3 inductances, which would theoretically account for 6 state electrical variables, the real state variables are 4, because of the node on the transversal branch: the Kirchhoff law imposes that the vector sum of the currents on the node is null and therefore the currents on the 3 inductances present a constraint to be fulfilled. The possible set of electrical state variables is composed of 5 vector elements or, equivalently, 10 scalar elements:

$$\boldsymbol{x}_{ext} = [i_{sD} \; i_{sQ} \; i_{rd} \; i_{rq} \; \psi_{sD} \; \psi_{sQ} \; \psi_{md} \; \psi_{mq} \; \psi_{rd} \; \psi_{rq}]. \quad (1)$$

The components of the vector $\boldsymbol{x}_{ext}$ are: the direct and quadrature components of the stator and rotor currents, and the stator, rotor and magnetizing flux linkages. In Eq. (1) they are expressed in the stator reference frame, but the conclusions are still valid in any reference frame in which the model is expressed. Among the above set of 10 potential scalar state variables, one possible set of state variables is that composed of the stator currents and the rotor flux linkages. Such a set is typically chosen as far as rotor flux oriented control is adopted. If the resistance R_0 accounting for the iron losses is considered, then the constraint linking together the currents in the 3 inductances is not valid any more. It implies that the
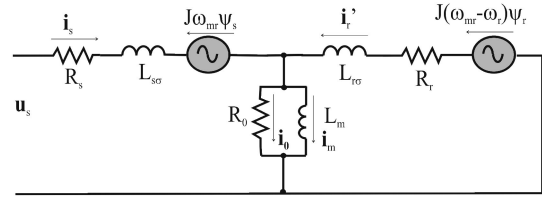

FIGURE 1. Electric scheme of the RIM dynamic model including iron losses in the rotor flux oriented reference frame.

electrical state variables increase from 4 to 6. Coherently with the above considerations on the rotor flux oriented control, considering that the iron losses depend on the three-phase magnetizing flux, the following set of state variables has been chosen to derive the proposed model:

$$\boldsymbol{x} = [i_{sD} \; i_{sQ} \; \psi_{md} \; \psi_{mq} \; \psi_{rd} \; \psi_{rq}]. \quad (2)$$

Such a set is typically chosen as far as rotor flux oriented control is adopted. According to the electric scheme of Fig. 1,[1] the stator and rotor space-vector equations of the induction machine expressed in the rotor flux oriented reference frame are the following:

$$\boldsymbol{u}_s^{\psi_r} = R_s \boldsymbol{i}_s^{\psi_r} + \frac{d\boldsymbol{\psi}_s^{\psi_r}}{dt} + j\omega_{mr}\boldsymbol{\psi}_s^{\psi_r}, \quad (3a)$$

$$0 = R_r \boldsymbol{i}_r^{\psi_r} + \frac{d\boldsymbol{\psi}_r^{\psi_r}}{dt} + j(\omega_{mr} - \omega_r)\boldsymbol{\psi}_r^{\psi_r}. \quad (3b)$$

The dynamic equation of the three-phase magnetizing flux is the following:

$$\frac{d\boldsymbol{\psi}_m^{\psi_r}}{dt} + j\omega_{mr}\boldsymbol{\psi}_m^{\psi_r} = R_0 \boldsymbol{i}_0^{\psi_r}, \quad (4)$$

where the relationships between fluxes and currents become:

$$\boldsymbol{\psi}_s^{\psi_r} = \boldsymbol{\psi}_m^{\psi_r} + L_{\sigma_s}\boldsymbol{i}_s^{\psi_r}, \quad (5a)$$

$$\boldsymbol{\psi}_r^{\psi_r} = \boldsymbol{\psi}_m^{\psi_r} + L_{\sigma_r}\boldsymbol{i}_r^{\psi_r}, \quad (5b)$$

$$\boldsymbol{\psi}_m^{\psi_r} = L_m \boldsymbol{i}_m^{\psi_r}, \quad (5c)$$

and the current balance on the node can be written as:

$$\boldsymbol{i}_s^{\psi_r} + \boldsymbol{i}_r^{\psi_r} = \boldsymbol{i}_m^{\psi_r} + \boldsymbol{i}_0^{\psi_r}. \quad (6)$$

In order to obtain the complete state-space model of the induction machine, the mechanical equation should be added. With this regards, it is well known [21] that the saturation does not affect the electromagnetic torque expression, but the value of the torque varies indirectly due to the variation of the stator current and rotor flux, besides the variation due to the magnetic parameters. Based on this consideration, the expression of the electromagnetic torque of RIM can be written as: $t_e = \frac{3}{2} p \frac{L_m}{L_r} \psi_{rx} i_{sy}$, where p is the number of pole pairs. The mechanical equation, applying the Newton's equation to a rotating mass with inertia moment J_m and viscous friction coefficient f_v, can be written as:

$$\dot{\omega}_r = -a_m \omega_r + b_m \left(\frac{3}{2} \frac{L_m}{L_r} \psi_{rx} i_{sy} - t_L \right), \quad (7)$$

[1]All variables in Fig. 1 are referred to an orthogonal reference frame synchronous to the rotor flux position.

where $a_m = \frac{f_v}{J_m}$, $b_m = \frac{p}{J_m}$ and t_L is the load torque.

A. IRON LOSSES EXPRESSION

In general, it can be stated that the iron core losses ΔP_{core} of a RIM can be divided in two terms, respectively the hysteresis and the eddy current losses, as follows:

$$\Delta P_{core\,hyst} = \alpha_z f B_p^z, \tag{8a}$$

$$\Delta P_{core\,eddy\,curr} = \beta_z f^2 B_p^2, \tag{8b}$$

where B_p is the peak value of the air-gap flux density, f is the fundamental supply frequency, z is the *Steinmetz* coefficient, α_z and β_z are coefficients depending on the material and on the flux density.

In the proposed model, the iron losses have represented in the space-vector electrical circuit of the RIM by means of a time varying resistance R_0 in the transversal branch. In classic models of the RIM including iron losses, R_0 is assumed constant, which implies a representation of the iron losses with a quadratic dependence from the air-gap flux density amplitude (proportional to the three-phase magnetizing flux amplitude) and pulsation. This assumption correctly represents the eddy current losses, while does not properly reproduce the hysteresis losses. In the adopted model, as in [14], [16], R_0 is assumed a variable quantity, in such a way to let both hysteresis and eddy current losses be reproduced correctly. Starting from the work [14], [16], the electric power dissipated at steady-state on R_0 can be written on the basis of the space-vector of the three-phase magnetizing flux as:

$$\begin{aligned}\Delta P_{iron} &= \Delta P_{core\,hyst} + \Delta P_{core\,eddy\,curr} \\ &= \frac{3}{2} \frac{k\omega_1 |\boldsymbol{\psi}_m^{\psi_r}|^z + \omega_1^2 |\boldsymbol{\psi}_m^{\psi_r}|^2}{R_{0t}},\end{aligned} \tag{9}$$

where R_{0t} is a constant resistance, k connotes the ratio between the eddy current and hysteresis power losses and ω_1 is supply pulsation of the machine. The power expression in (9) can be hardly used in transient working conditions, since ω_1 in transient is meaningless. On the contrary, the expression of the back-electromotive force $\frac{d\boldsymbol{\psi}_m^{\psi_r}}{dt}$ can be exploited, leading to the following expression of a time varying R_0:

$$R_0 = \frac{2}{3} \frac{R_{0t}}{1 + k\omega_1 |\boldsymbol{\psi}_m^{\psi_r}|^{z-1}/\frac{d\boldsymbol{\psi}_m^{\psi_r}}{dt}}. \tag{10}$$

Eq. (10) can be deduced after expressing the active power due to the iron losses, whose formulation is given by the Steinmetz equations in eq. Eq. (9), as equal to the active power dissipated in the resistance R_0 of the space-vector equivalent circuit of the induction motor in Fig. 1. As a result, exploiting the space-vector equation describing the dynamics of the three-phase magnetizing flux, the equivalent expression of R_0 can be deduced. The entire derivation of Eq. (10) has been provided in [14], [16].

III. SATURATION OF THE IRON CORE

As for the description of the magnetic saturation of the iron core, two approaches are possible:

- defining current versus flux functions and consequently inductance versus flux functions;
- defining flux versus current functions and consequently inductance versus current functions.

In the following, both approaches will be developed, leading to original formulations of the magnetic characteristics of the RIM fulfilling the reciprocity conditions.

A. APPROACH 1: CURRENT VERSUS FLUX

This approach is based on the definition of suitable current versus flux functions. The effect of the load on the magnetic saturation has been considered here including both the rotor and the stator leakage fluxes (not equal in case of adoption of the T circuital scheme).

The following functions have been thus defined:

$$\begin{aligned}|\boldsymbol{i}_m^{\psi_r}| = \frac{|\boldsymbol{\psi}_m^{\psi_r}|}{L_{mu}} &\left(1 + \alpha_1 |\boldsymbol{\psi}_m^{\psi_r}|^{a_1} + \frac{\epsilon_1 L_{mu}}{d_1+2} |\boldsymbol{\psi}_m^{\psi_r}|^{c_1} |\boldsymbol{\psi}_{\sigma_r}^{\psi_r}|^{d_1+2} \right. \\ &\left. + \frac{\delta_1 L_{mu}}{d_1+2} |\boldsymbol{\psi}_m^{\psi_r}|^{c_1} |\boldsymbol{\psi}_{\sigma_s}^{\psi_r}|^{d_1+2} \right),\end{aligned} \tag{11a}$$

$$\begin{aligned}|\boldsymbol{i}_r^{\psi_r}| = \frac{|\boldsymbol{\psi}_{\sigma_r}^{\psi_r}|}{L_{\sigma_r u}} &\left(1 + \beta_1 |\boldsymbol{\psi}_{\sigma_r}^{\psi_r}|^{b_1} + \frac{\epsilon_1 L_{\sigma_r u}}{c_1+2} |\boldsymbol{\psi}_m^{\psi_r}|^{c_1+2} |\boldsymbol{\psi}_{\sigma_r}^{\psi_r}|^{d_1} \right. \\ &\left. + \frac{\xi_1 L_{\sigma_r u}}{e_1+2} |\boldsymbol{\psi}_{\sigma_r}^{\psi_r}|^{f_1} |\boldsymbol{\psi}_{\sigma_s}^{\psi_r}|^{e_1+2} \right),\end{aligned} \tag{11b}$$

$$\begin{aligned}|\boldsymbol{i}_s^{\psi_r}| = \frac{|\boldsymbol{\psi}_{\sigma_s}^{\psi_r}|}{L_{\sigma_s u}} &\left(1 + \gamma_1 |\boldsymbol{\psi}_{\sigma_s}^{\psi_r}|^{b_1} + \frac{\delta_1 L_{\sigma_s u}}{c_1+2} |\boldsymbol{\psi}_m^{\psi_r}|^{c_1+2} |\boldsymbol{\psi}_{\sigma_s}^{\psi_r}|^{d_1} \right. \\ &\left. + \frac{\xi_1 L_{\sigma_s u}}{e_1+2} |\boldsymbol{\psi}_{\sigma_s}^{\psi_r}|^{f_1} |\boldsymbol{\psi}_{\sigma_r}^{\psi_r}|^{e_1+2} \right),\end{aligned} \tag{11c}$$

where $\{\alpha_1, \beta_1, \gamma_1, \delta_1, \epsilon_1, \xi_1\}$ and $\{a_1, b_1, c_1, d_1, e_1, f_1\}$ are two set of positive parameters characterizing the entire magnetic model of the machine. The proposed magnetic model requires, therefore, 15 parameters to be properly described. Starting from Eq.s (11), it can be verified that the dynamic inductances (their inverse) fulfill the reciprocity conditions:

$$\tilde{L}_{m\sigma_s}^{-1} = \frac{d|\boldsymbol{i}_m^{\psi_r}|}{d|\boldsymbol{\psi}_{\sigma_s}^{\psi_r}|} = \frac{d|\boldsymbol{i}_s^{\psi_r}|}{d|\boldsymbol{\psi}_m^{\psi_r}|} = \delta_1 |\boldsymbol{\psi}_m^{\psi_r}|^{c_1+1} |\boldsymbol{\psi}_{\sigma_s}^{\psi_r}|^{d_1+1}, \tag{12a}$$

$$\tilde{L}_{m\sigma_r}^{-1} = \frac{d|\boldsymbol{i}_r^{\psi_r}|}{d|\boldsymbol{\psi}_m^{\psi_r}|} = \frac{d|\boldsymbol{i}_m^{\psi_r}|}{d|\boldsymbol{\psi}_{\sigma_r}^{\psi_r}|} = \epsilon_1 |\boldsymbol{\psi}_m^{\psi_r}|^{c_1+1} |\boldsymbol{\psi}_{\sigma_r}^{\psi_r}|^{d_1+1}, \tag{12b}$$

$$\tilde{L}_{\sigma_s\sigma_r}^{-1} = \frac{d|\boldsymbol{i}_r^{\psi_r}|}{d|\boldsymbol{\psi}_{\sigma_s}^{\psi_r}|} = \frac{d|\boldsymbol{i}_s^{\psi_r}|}{d|\boldsymbol{\psi}_{\sigma_r}^{\psi_r}|} = \xi_1 |\boldsymbol{\psi}_{\sigma_s}^{\psi_r}|^{f_1+1} |\boldsymbol{\psi}_{\sigma_r}^{\psi_r}|^{e_1+1}. \tag{12c}$$

The expressions of the static inductances versus fluxes can be thus derived as follows:

$$L_m = \frac{|\boldsymbol{\psi}_m^{\psi_r}|}{|\boldsymbol{i}_m^{\psi_r}|} = \frac{L_{mu}}{g_1(\boldsymbol{\psi}_m^{\psi_r}, \boldsymbol{\psi}_{\sigma_s}^{\psi_r}, \boldsymbol{\psi}_{\sigma_r}^{\psi_r})} \tag{13a}$$

$$L_{\sigma_r} = \frac{|\boldsymbol{\psi}_{\sigma_r}^{\psi_r}|}{|\boldsymbol{i}_r^{\psi_r}|} = \frac{L_{\sigma_r u}}{g_2(\boldsymbol{\psi}_m^{\psi_r}, \boldsymbol{\psi}_{\sigma_s}^{\psi_r}, \boldsymbol{\psi}_{\sigma_r}^{\psi_r})} \tag{13b}$$

$$L_{\sigma_s} = \frac{|\boldsymbol{\psi}_{\sigma_s}^{\psi_r}|}{|\boldsymbol{i}_s^{\psi_r}|} = \frac{L_{\sigma_s u}}{g_3(\boldsymbol{\psi}_m^{\psi_r}, \boldsymbol{\psi}_{\sigma_s}^{\psi_r}, \boldsymbol{\psi}_{\sigma_r}^{\psi_r})} \tag{13c}$$

where:

$$g_1(\boldsymbol{\psi}_m^{\psi_r}, \boldsymbol{\psi}_{\sigma_s}^{\psi_r}, \boldsymbol{\psi}_{\sigma_r}^{\psi_r}) = 1 + \alpha_1 |\boldsymbol{\psi}_m^{\psi_r}|^{a_1}$$
$$+ \frac{\epsilon_1 L_{mu}}{d_1 + 2} |\boldsymbol{\psi}_m^{\psi_r}|^{c_1} |\boldsymbol{\psi}_{\sigma_r}^{\psi_r}|^{d_1+2} + \frac{\delta_1 L_{mu}}{d_1 + 2} |\boldsymbol{\psi}_m^{\psi_r}|^{c_1} |\boldsymbol{\psi}_{\sigma_s}^{\psi_r}|^{d_1+2},$$
(14a)

$$g_2(\boldsymbol{\psi}_m^{\psi_r}, \boldsymbol{\psi}_{\sigma_s}^{\psi_r}, \boldsymbol{\psi}_{\sigma_r}^{\psi_r}) = 1 + \beta_1 |\boldsymbol{\psi}_{\sigma_r}^{\psi_r}|^{b_1}$$
$$+ \frac{\epsilon_1 L_{\sigma_r u}}{c_1 + 2} |\boldsymbol{\psi}_m^{\psi_r}|^{c_1+2} |\boldsymbol{\psi}_{\sigma_r}^{\psi_r}|^{d_1} + \frac{\xi_1 L_{\sigma_r u}}{e_1 + 2} |\boldsymbol{\psi}_{\sigma_r}^{\psi_r}|^{f_1} |\boldsymbol{\psi}_{\sigma_s}^{\psi_r}|^{e_1+2},$$
(14b)

$$g_3(\boldsymbol{\psi}_m^{\psi_r}, \boldsymbol{\psi}_{\sigma_s}^{\psi_r}, \boldsymbol{\psi}_{\sigma_r}^{\psi_r}) = 1 + \gamma_1 |\boldsymbol{\psi}_{\sigma_s}^{\psi_r}|^{b_1}$$
$$+ \frac{\delta_1 L_{\sigma_s u}}{c_1 + 2} |\boldsymbol{\psi}_m^{\psi_r}|^{c_1+2} |\boldsymbol{\psi}_{\sigma_s}^{\psi_r}|^{d_1} + \frac{\xi_1 L_{\sigma_s u}}{e_1 + 2} |\boldsymbol{\psi}_{\sigma_s}^{\psi_r}|^{f_1} |\boldsymbol{\psi}_{\sigma_r}^{\psi_r}|^{e_1+2}.$$
(14c)

Among the 15 parameters whose knowledge is required by this approach, the only ones presenting a precise physical meaning are L_{mu}, $L_{\sigma_r u}$, $L_{\sigma_s u}$. They represent, respectively, the values of the three-phase magnetizing inductance, the rotor leakage inductance and the stator leakage inductance, obtained for null values of the three-phase magnetizing flux, rotor leakage flux and stator leakage flux. The above described current versus flux approach is clearly inspired to [13], while being the part of the model related to the cross saturation entirely original, because of the assumption of validity of the T circuital scheme.

B. APPROACH 2: FLUX VERSUS CURRENT

This approach is based on the definition of suitable flux versus current functions. As recalled above, the effect of the load on the magnetic saturation has been considered here including both the rotor and the stator currents (not equal in case of adoption of the T circuital scheme). The following functions have been thus defined:

$$|\boldsymbol{\psi}_m^{\psi_r}| = \alpha_2 \left(1 - e^{-a_2 |\boldsymbol{i}_m^{\psi_r}|}\right) + \beta_2 |\boldsymbol{i}_m^{\psi_r}|$$
$$+ \gamma_2 \frac{2 - e^{-b_2 |\boldsymbol{i}_m^{\psi_r}||\boldsymbol{i}_r^{\psi_r}|} - e^{-c_2 |\boldsymbol{i}_m^{\psi_r}||\boldsymbol{i}_s^{\psi_r}|}}{|\boldsymbol{i}_m^{\psi_r}|},$$
(15a)

$$|\boldsymbol{\psi}_{\sigma_r}^{\psi_r}| = \delta_2 \left(1 - e^{-e_2 |\boldsymbol{i}_r^{\psi_r}|}\right) + \epsilon_2 |\boldsymbol{i}_r^{\psi_r}|$$
$$+ \gamma_2 \frac{2 - e^{-b_2 |\boldsymbol{i}_m^{\psi_r}||\boldsymbol{i}_r^{\psi_r}|} - e^{-d_2 |\boldsymbol{i}_r^{\psi_r}||\boldsymbol{i}_s^{\psi_r}|}}{|\boldsymbol{i}_r^{\psi_r}|},$$
(15b)

$$|\boldsymbol{\psi}_{\sigma_s}^{\psi_r}| = \eta_2 \left(1 - e^{-f_2 |\boldsymbol{i}_s^{\psi_r}|}\right) + \xi_2 |\boldsymbol{i}_s^{\psi_r}|$$
$$+ \gamma_2 \frac{2 - e^{-c_2 |\boldsymbol{i}_m^{\psi_r}||\boldsymbol{i}_s^{\psi_r}|} - e^{-d_2 |\boldsymbol{i}_r^{\psi_r}||\boldsymbol{i}_s^{\psi_r}|}}{|\boldsymbol{i}_s^{\psi_r}|},$$
(15c)

where $\{\alpha_2, \beta_2, \gamma_2, \delta_2, \epsilon_2, \xi_2, \eta_2\}$ and $\{a_2, b_2, c_2, d_2, e_2, f_2\}$ are two set of positive parameters characterizing the entire magnetic model of the machine. Note that flux versus current functions must exhibit a certain kind of waveform, in particular the classic saturation shape. For high values of the current, the flux must slightly increase. For zero values of the current,

a minimal residual flux must be present in the machine. Therefore the functions adopted in (15) have been purposely created in order to respect these physical constraints.

The proposed magnetic model requires, therefore, 13 parameters to be properly described. Starting from Eqs (15), it can be verified that the dynamic inductances fulfill the reciprocity conditions:

$$\tilde{L}_{m\sigma_s} = \frac{d|\boldsymbol{\psi}_{\sigma_s}^{\psi_r}|}{d|\boldsymbol{i}_m^{\psi_r}|} = \frac{d|\boldsymbol{\psi}_m^{\psi_r}|}{d|\boldsymbol{i}_s^{\psi_r}|} = \gamma_2 c_2 e^{-c_2 |\boldsymbol{i}_m^{\psi_r}||\boldsymbol{i}_s^{\psi_r}|},$$
(16a)

$$\tilde{L}_{m\sigma_r} = \frac{d|\boldsymbol{\psi}_m^{\psi_r}|}{d|\boldsymbol{i}_r^{\psi_r}|} = \frac{d|\boldsymbol{\psi}_{\sigma_r}^{\psi_r}|}{d|\boldsymbol{i}_m^{\psi_r}|} = \gamma_2 b_2 e^{-b_2 |\boldsymbol{i}_m^{\psi_r}||\boldsymbol{i}_r^{\psi_r}|},$$
(16b)

$$\tilde{L}_{\sigma_s \sigma_r} = \frac{d|\boldsymbol{\psi}_{\sigma_s}^{\psi_r}|}{d|\boldsymbol{i}_r^{\psi_r}|} = \frac{d|\boldsymbol{\psi}_{\sigma_r}^{\psi_r}|}{d|\boldsymbol{i}_s^{\psi_r}|} = \gamma_2 d_2 e^{-d_2 |\boldsymbol{i}_r^{\psi_r}||\boldsymbol{i}_s^{\psi_r}|}.$$
(16c)

Eq.s (16) represent the dynamic inductances of the RIM.

The expressions of the static inductances versus currents can be thus derived as follows:

$$L_m = \frac{|\boldsymbol{\psi}_m^{\psi_r}|}{|\boldsymbol{i}_m^{\psi_r}|} = \alpha_2 \frac{\left(1 - e^{-a_2 |\boldsymbol{i}_m^{\psi_r}|}\right)}{|\boldsymbol{i}_m^{\psi_r}|} + \beta_2$$
$$+ \gamma_2 \frac{2 - e^{-b_2 |\boldsymbol{i}_m^{\psi_r}||\boldsymbol{i}_r^{\psi_r}|} - e^{-c_2 |\boldsymbol{i}_m^{\psi_r}||\boldsymbol{i}_s^{\psi_r}|}}{|\boldsymbol{i}_m^{\psi_r}|^2},$$
(17a)

$$L_{\sigma r} = \frac{|\boldsymbol{\psi}_{\sigma_r}^{\psi_r}|}{|\boldsymbol{i}_r^{\psi_r}|} = \delta_2 \frac{\left(1 - e^{-e_2 |\boldsymbol{i}_r^{\psi_r}|}\right)}{|\boldsymbol{i}_r^{\psi_r}|} + \epsilon_2$$
$$+ \gamma_2 \frac{2 - e^{-b_2 |\boldsymbol{i}_m^{\psi_r}||\boldsymbol{i}_r^{\psi_r}|} - e^{-d_2 |\boldsymbol{i}_r^{\psi_r}||\boldsymbol{i}_s^{\psi_r}|}}{|\boldsymbol{i}_r^{\psi_r}|^2},$$
(17b)

$$L_{\sigma s} = \frac{|\boldsymbol{\psi}_{\sigma_s}^{\psi_r}|}{|\boldsymbol{i}_s^{\psi_r}|} = \eta_2 \frac{\left(1 - e^{-f_2 |\boldsymbol{i}_s^{\psi_r}|}\right)}{|\boldsymbol{i}_s^{\psi_r}|} + \xi_2$$
$$+ \gamma_2 \frac{2 - e^{-c_2 |\boldsymbol{i}_m^{\psi_r}||\boldsymbol{i}_s^{\psi_r}|} - e^{-d_2 |\boldsymbol{i}_r^{\psi_r}||\boldsymbol{i}_s^{\psi_r}|}}{|\boldsymbol{i}_s^{\psi_r}|^2}.$$
(17c)

It can be noticed that the coefficients α_2, a_2 and β_2 (analogously δ_2, e_2 and ϵ_2 for the rotor leakage inductance and η_2, f_2 and ξ_2 for the stator leakage inductance) can be physically interpreted. For example, considering that $\lim_{|\boldsymbol{i}_m^{\psi_r}| \to 0} L_m = \alpha_2 a_2 + \beta_2$ and $\lim_{|\boldsymbol{i}_m^{\psi_r}| \to \infty} L_m = \beta_2$, β_2 can be interpreted as the self-inductance when the machine is fully saturated, and the relation $\alpha_2 a_2 + \beta_2$ as the tangent of the magnetizing curve at the origin, which represents the inductance corresponding to the residual magnetization of the iron core. For more details about these kind of physical interpretations the reader is addressed to [22], [23].

IV. GA-BASED OFF-LINE PARAMETER ESTIMATION METHOD

Since the RIM magnetic fluxes are not measurable quantities, not all of the parameters appearing in the space-vector state model of the induction motor can be directly obtained. On the contrary, they can be identified by means of a convenient identification technique. As for the identifiability issue,

in [20], [24] it is shown that all 4 electrical parameters of the classic RIM model can be identified if a speed transient is exploited, while in sinusoidal steady-state conditions, on the contrary, only 1 electrical parameter can be estimated. The parameter estimation technique proposed in this paper is based on a specific space-vector model of the RIM, described by the space-vector equations from (3) to (6). In such a model, however, the magnetic saturation effect has been mathematically described with two different approaches, respectively the current versus flux approach (approach 1) and the flux versus current approach (approach 2). The adoption of any of the two approaches implies the identification of a different set of parameters describing the magnetic behavior of the machine (respectively 15 in approach 1 and 13 in approach 2). As for the equations describing the dynamic model, it can be observed that its number increases from 4 scalar equations of the classic model to 6 scalar equations of the proposed one, permitting the estimation of an increased number of parameters. In the case under study, the chosen vector $\boldsymbol{w}$ of the parameters to be estimated varies, according to the approach followed for the description of the magnetic behavior of the machine. The number of parameters to be estimated is very high, in particular 18 with approach 1 (15 related to the magnetic behavior plus R_s, R_r and R_{0t}) and 16 with approach 2 (13 related to the magnetic behavior plus R_s, R_r and R_{0t}). Among these parameters, the stator resistance R_s is not assumed as a quantity to be estimated, since it can be easily measured with simple voltage/current measurements. As for the parameters describing the magnetic behaviour of the machine, the following simplifying assumptions have been made, in order to make the set of parameters estimated on the basis of dynamic tests.

Since the number of parameters to be estimated is very high compared with the number of equations available, some simplifying assumption has to be made. In particular, as for approach 1, the following assumptions have been made. The parameters L_{mu}, $L_{\sigma_s u}$, $L_{\sigma_r u}$, α_1, β_1, δ_1 and a_1, b_1, c_1, d_1 have been directly estimated on the basis of the proposed algorithm; it has been then assumed that $\gamma_1 = \beta_1$, $\epsilon_1 = \xi_1 = \delta_1$ and $e_1 = f_1 = d_1$. It should be noted that the considered saturation model is absolutely general, meaning that all parameters could theoretically be different. As a matter of fact, it is reasonable to assume that some of them are equal for two reasons. The first reason is that they are related to cross saturation effects, which plays a minor role with respect to self-saturation effect. The second reason is that it is reasonable to assume that the coefficients on the stator and rotor terms are almost equal. Finally, increasing the number of parameters to be estimated increases significantly the complexity of the identification process. For these reasons, the above reasonable simplifications have been made. The final vector of the parameters to be estimated with approach 1 is composed by the following 12 elements:

$$\boldsymbol{w}_1 = [L_{mu}, \ L_{\sigma_s u}, \ L_{\sigma_r u}, \ R_r, \ R_{0t}, \ \alpha_1, \ \beta_1, \ \delta_1, \ a_1, \ b_1, \ c_1, \ d_1]. \tag{18}$$
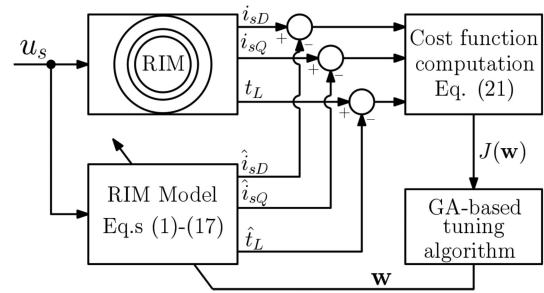

FIGURE 2. Block diagram of the RIM parameter estimation technique.

As for approach 2, the following assumptions have been made. The α_2, β_2, γ_2, δ_2, ϵ_2, a_2, b_2, c_2, d_2 and f_2 have been directly estimated on the basis of the proposed algorithm; it has been then assumed that $\eta_2 = \delta_2$, $\xi_2 = \epsilon_2$ and $e_2 = f_2$. The final vector of the parameters to be estimated with approach 2 is composed by the following 12 elements:

$$\boldsymbol{w}_2 = [R_r, \ R_{0t}, \ \alpha_2, \ \beta_2, \ \gamma_2, \ \delta_2, \ \epsilon_2, \ a_2, \ b_2, \ c_2, \ d_2, \ f_2]. \tag{19}$$

To identify the parameters of the model (3)-(17), separately with approaches 1 and 2, a suitable method is used, which can be formulated as follows. The RIM has been supplied in order to perform a set of speed transients; at each value of speed steady-state, several load torques have been given to the RIM drive and finally, for each load condition, several magnetization levels have been tested (corresponding to different values of the rotor flux linkage references). In this way, the working space composed of speed, load torque and reference rotor flux can be covered suitably for parameter estimation. The stator voltages and currents and the load torque acquired during the above tests have been recorded. Afterwards, the space-vector state model (3)-(17) has been supplied numerically with the same values of stator voltages adopted in the experimental test, and the stator currents and the load torque have been computed by the model (3)-(17). Finally, the difference between the measured stator currents and torque and the corresponding ones estimated by the model have been exploited to recursively tune the values of the model's parameters, until when the outputs of the model match the corresponding ones of the real RIM. Note that the load torque at steady state is equal to the electromagnetic torque generated by the motor, therefore the use of this variable for estimating the model parameters is very important because it takes into account the effective magnetization level of the machine, since the torque depends both from currents and from rotor flux ad shown in Eq. (7). Fig. 2 sketches the block diagram of the technique adopted for the parameter estimation of the RIM.

As for the tuning algorithm in Fig. 2, the following technique has been adopted. Given a set of N data pairs of independent and dependent vector variables, $\{(\boldsymbol{z}_i, \boldsymbol{y}_i), \ i = 1, \ldots, N\}$, find the parameter vector $\boldsymbol{w}$ of the model curve $\boldsymbol{g}(\boldsymbol{z}, \boldsymbol{w})$ so as to minimize the root square of the sum of the

squares of the deviations given by:

$$J(\boldsymbol{w}) = \frac{1}{N}\sqrt{\sum_{i=1}^{N}(y_i - \boldsymbol{g}(z, \boldsymbol{w}))^2}. \qquad (20)$$

In the case of the RIM parameter estimation, a Genetic Algorithm (GA) [19] has been used, which provides a numerical solution to the problem of minimizing a non-linear function over a space of parameters of the function itself. In particular, the parameter vector $\boldsymbol{w}$ is the above cited set of the electrical parameters to be estimated, and the function to be minimized is:

$$J(\boldsymbol{w}) =$$
$$\frac{1}{N}\sqrt{\sum_{i=1}^{N}\left(i_{sD} - \hat{i}_{sD}\right)^2 + \sum_{i=1}^{N}\left(i_{sQ} - \hat{i}_{sQ}\right)^2 + \sum_{i=1}^{N}\left(t_L - \hat{t}_L\right)^2},$$
$$(21)$$

where N is the total number of samples supplied to the algorithm, i_{sD}, i_{sQ} and t_L are the measured direct and quadrature components of the stator currents and the load torque, $\hat{i}_{sD}$, $\hat{i}_{sQ}$ and $\hat{t}_L$ are the corresponding quantities computed by means of the mathematical model (3)-(17) using the computed values of the parameters, in correspondence to the same values of supply voltage used to obtain i_{sD}, i_{sQ} and t_L. Note that in order to obtain the estimated value of load torque $\hat{t}_L$ it is possible to consider the extended 2th-order mechanical model of the machine composed by equation (7) and the extra state equation $\dot{\hat{t}}_L = 0$. Then, it is possible to design an high-gain observer as described in [25, Chapter 14.5], which can estimate both mechanical speed and load torque. The observer is sourced by the values of stator current and rotor flux, and the error between the estimated and measured speed is used as driven term. The reader can refer to [25] for further details.

The adoption of GAs allows avoiding the problem of the local minima, since genetic algorithms are evolutionary optimization algorithms robust versus the initial condition. In any case, also if the initial condition does not affect the final solution, a good initial choice accelerates the convergence speed of the algorithm. For this reason, the methodology has been tested starting from a set of electrical parameters which can be considered an initial good guess and are computed directly from the name-plate data of the machine. For the case under study, some typical rated data valid for RIMs of the same size have been employed to compute the initial set of parameters (rated efficiency 70%, rated slip 20%).

However, since the initial condition computed from the name-plate data of the machine can be very different to the real parameter, the searching domain has to be chosen sufficiently large, and this lead to very long computational time because of the high number of parameters to be estimated. For this reason a purposely devised has been used in order to explore a wider domain of possible solutions and contemporary to guarantee a restrained computational time for the algorithm. In particular, the identification procedure has been divided in two steps. As for first step, only some *main parameters* have been estimated, where for *main parameters* we mean the parameters that mainly affect the behavior of the model, and the

other parameters have been fixed equal to the initial choices computed from the name-plate data of the machine. For example, for approach 1, in the first step the estimated quantities have been only $[L_{mu}, R_r, R_{0t}, \alpha_1, \beta_1, a_1, b_1]$, while $[L_{\sigma_s u}, L_{\sigma_r u}, \delta_1, c_1, d_1]$ have been kept constant. During this first step the lower and upper bounds of the sets where the algorithm search the possible parameters have been chosen expressly large in order to investigate a bigger domain of possible solutions. The GA has been implemented using the optimization tool in MATLAB, and in this step 1 the population size and the number of iterations have been chosen small in order to guarantee a small computational time, in particular the population size adopted was composed of 20 individuals, and the algorithm is stopped after 10 iterations. As for approach 1, the results of this first step gives the following values as for the parameters' vector:

$$\boldsymbol{w}_{01} = [0.2,\ 6.2 \cdot 10^{-3},\ 1.2 \cdot 10^{-3},$$
$$1.8,\ 10^3,\ 2,\ 2,\ 0.1,\ 1,\ 1,\ 1,\ 1]. \qquad (22)$$

Afterwards, as second step, the whole parameters vector has been considered, but using as initial condition the result of the first step given in Eq. (22). In this second step the population size and the number of iterations have been increased because of the higher number of parameters, in particular the population size adopted was composed of 50 individuals, and the algorithm is stopped after 20 iterations. On the contrary, in this second step, the searching domain has been suitably reduced in order to ensure a faster convergence time.

As for approach 2, the same procedure described above have been used, but by considering as *main parameters* the following: $[R_r,\ R_{0t},\ \alpha_2,\ \beta_2,\ \delta_2,\ a_2,\ f_2]$, while $[\gamma_2,\ \epsilon_2,\ b_2,\ c_2,\ d_2]$ have been kept constant. As for approach 2, the results of the first step gives the following value as for the parameters' vector:

$$\boldsymbol{w}_{02} = [1,\ 10^3,\ 2,\ 0.2,\ 0.05,\ 0.3,\ 0.2,\ 1,\ 2,\ 1,\ 1,\ 1]. \qquad (23)$$

This parameters' vector will be considered as initial choice for the final identification carried out in the second step. Also for approach 2 the population size adopted at step 2 was composed of 50 individuals, and the algorithm is stopped after 20 iterations.

With reference to the other GA parameters, the following choice has been made for both approaches and for both steps: a) mutation function: constraint dependent; b) crossover function: scattered; c) selection function: stochastic uniform; d) elite count: 5% of the population size; e) crossover fraction: 0.8. See [19] for details about the use of the genetic algorithms.

Moreover, another purposely devised method have been used during the identification procedure. In particular, for both approaches some parameters have been normalized by means of constant scalars so that all parameters range in comparable sets of values. For example as for approach 1 the following rescaled vector has been used instead of (18):

$$\bar{\boldsymbol{w}}_1 = [L_{mu} \cdot 10^{-1},\ L_{\sigma_s u} \cdot 10^{-3},\ L_{\sigma_r u} \cdot 10^{-3},\ R_r,$$
$$R_{0t} \cdot 10^3,\ \alpha_1,\ \beta_1,\ \delta_1 \cdot 10^{-1},\ a_1,\ b_1,\ c_1,\ d_1], \qquad (24)$$

TABLE 1. Rated Data and Main Parameters of the Induction Motor

Rated power, P_{rated}	2.2 kW
Rated voltage, V_{rated}	220 V
Rated current, I_{rated}	4.8 A
Rated frequency, f_{rated}	50 Hz
Rated speed, ω_{rated}	149.75 rad/s
Pole-pairs	2
Moment of inertia, J_m	0.0048 Nms^2
Viscous friction coefficient, f_v	0.0023 N m s
Stator resistance, R_s	2.9 Ω
Rotor resistance, R_r	1.52 Ω
Stator inductance, L_s	223 mH
Rotor inductance, L_r	229 mH
3-phase magnetizing inductance, L_m	217 mH

while as for approach 2 the following rescaled vector has been used instead of (19):

$$\bar{w}_2 = [R_r, \ R_{0t} \cdot 10^3, \ \alpha_2, \ \beta_2 \cdot 10^{-1}, \ \gamma_2 \cdot 10^{-2},$$

$$\delta_2 \cdot 10^{-1}, \ \epsilon_2 \cdot 10^{-1}, \ a_2, \ b_2, \ c_2, \ d_2, \ f_2]. \quad (25)$$

With choices (24) and (25) the the following vectors of initial values have been adopted for the final identification carried out in the second step instead of (22)–(23):

$$\bar{w}_{01} = [2, \ 6.2, \ 1.2, \ 1.8, \ 1, \ 2, \ 2, \ 1, \ 1, \ 1, \ 1, \ 1], \quad (26)$$

$$\bar{w}_{02} = [1, \ 1, \ 2, \ 2, \ 5, \ 3, \ 2, \ 1, \ 2, \ 1, \ 1, \ 1]. \quad (27)$$

The above described rescaling is very important in order to ensure a faster and more efficient convergence and it represents a good practice in many numerical algorithm such as GA.

The above described procedure ensures a sufficiently wide searching domain, at least for the parameters that mainly affect the behavior of the model, and contemporary the computational time is restrained because the searching domain is reduced when the whole parameters vector has been considered during the second step. From the experimental results shown in the next section it will be shown that the above described procedure leads to a good choice of the model's parameters ensuring a small value of the cost function (21).

V. TEST SET-UP

A test set-up composed of a 2.2 kW three phase induction motor drive supplied by a VSI-IGBT inverter has been used to perform the experimental tests. The adopted VSI power devices are IGBTs Semikron SKM 50GB123D. The induction motor parameters are listed in Table 1. The PWM technique has been set with a switching frequency of 5 kHz and the dead-time imposed at the modulator of the inverter is 2 μs. The RIM drive has been implemented a rotor flux oriented control. The control algorithm has been implemented on a DSpace DS1103 board. The sampling time of the entire control system has been set to 10 kHz. The RIM is mechanically coupled permanent magnet synchronous motor (PMSM), behaving as active load. The load torque is actively regulated by giving proper torque references to the PMSM drive. The input power measurements needed for the efficiency evaluation have been performed by using a Yokogawa WT3000 power meter (having a bandwidth of 1 MHz) which is able to correctly measure three phase powers also in distorted conditions. Output power has been
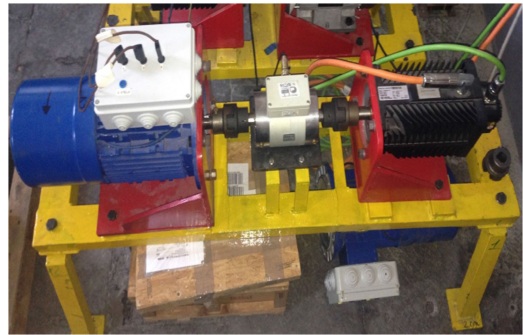
FIGURE 3. Photograph of the experimental test set-up.
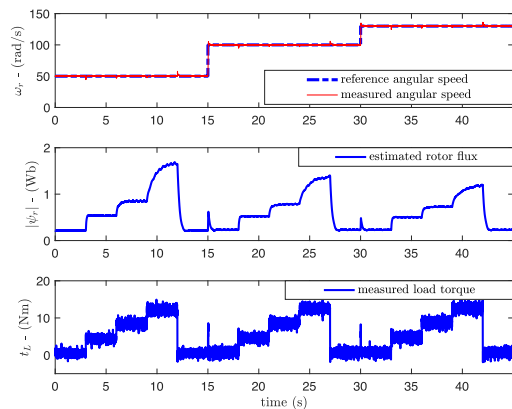
FIGURE 4. Rotor speed, rotor flux, load torque during test at variable flux and variable load torque (experiment).

directly computed on the basis of the speed measurement by an incremental encoder integrated on the RIM and electromagnetic torque measurement by means of a torquemeter model Himmelstein 59003V(4-2)-N-F-N-L-K. In particular, power efficiency is measured by a direct measurement method, it is calculated as the ratio between output and input power. Fig. 3 shows the photograph of the test rig.

VI. EXPERIMENTAL VALIDATION OF THE PARAMETERS IDENTIFICATION TECHNIQUE

On the basis of the above mentioned identification criteria necessary for the complete estimation of the set of parameters, the following experimental test has been made. The RIM drive has been given a set of subsequent speed steps of the type $50 \rightarrow 100 \rightarrow 130$ rad/s (ranging from medium/low to rated speed). At each speed, the drive has been given a set of load torque steps of the type $0 \rightarrow 4 \rightarrow 8 \rightarrow 12$ Nm. In order to make the RIM work at different magnetization levels for each set of speed/load, such test has been performed at variable flux corresponding to the maximum RIM efficiency for each speed/load; to do that the ELMT (Electrical Losses Minimization Technique) in [26] has been adopted.

Fig. 4 shows the RIM speed, the load torque and the rotor flux amplitudes during the test, while in Fig. 5 the corresponding waveforms of stator current components i_{sx} and i_{sy} are shown. These waveforms have been acquired in order to carry out the off-line procedure described in Section IV. Note
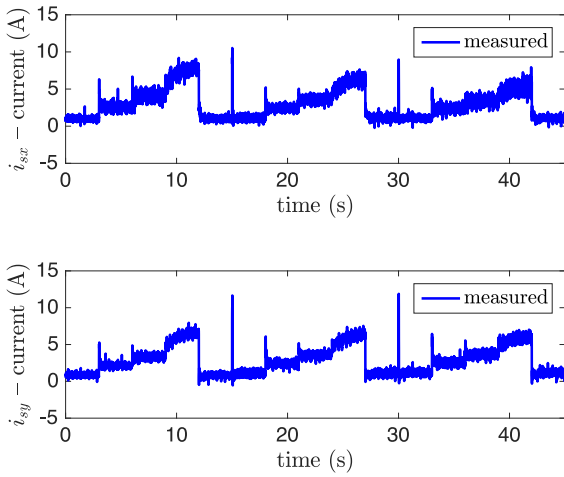
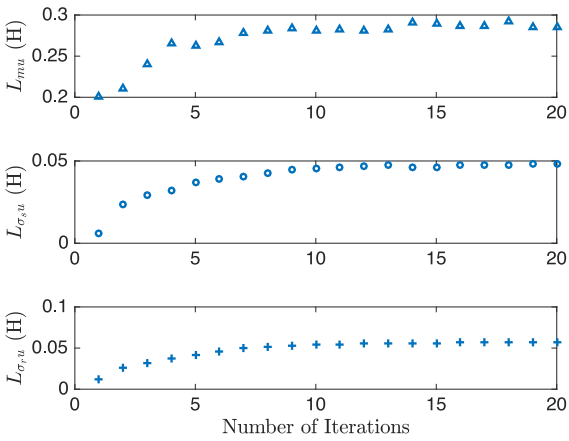**FIGURE 5. Stator current components i_{sD} and i_{sq} during test at variable flux and variable load torque (experiment).**

FIGURE 6. Convergence of the estimated parameters L_{mu}, $L_{\sigma_s u}$ and $L_{\sigma_r u}$ with approach 1 (experiment).
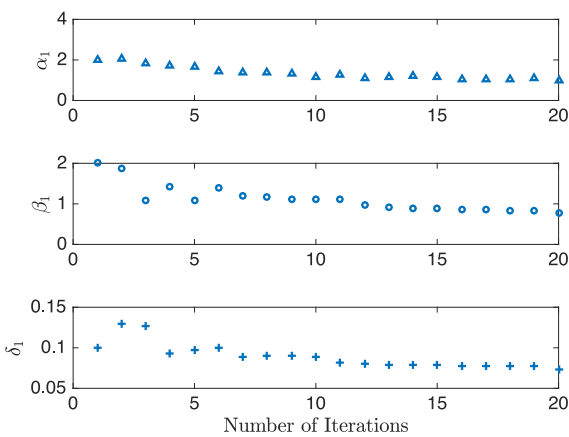
FIGURE 7. Convergence of the estimated parameters α_1, β_1 and δ_1 with approach 1 (experiment).
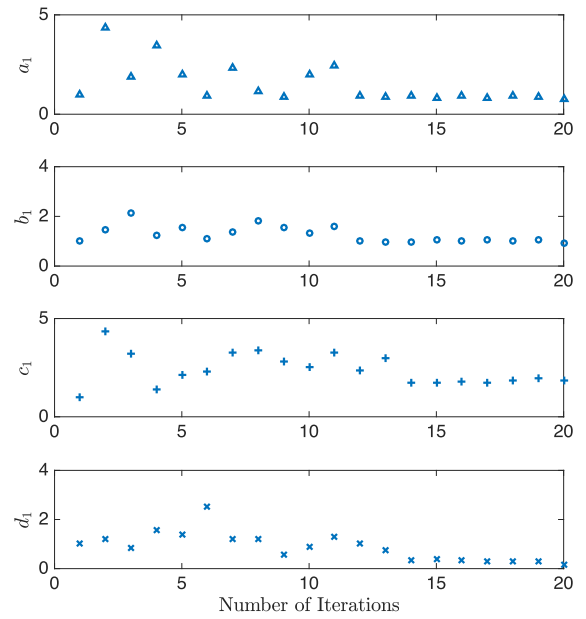
FIGURE 8. Convergence of the estimated parameters a_1, b_1, c_1 and d_1 with approach 1 (experiment).
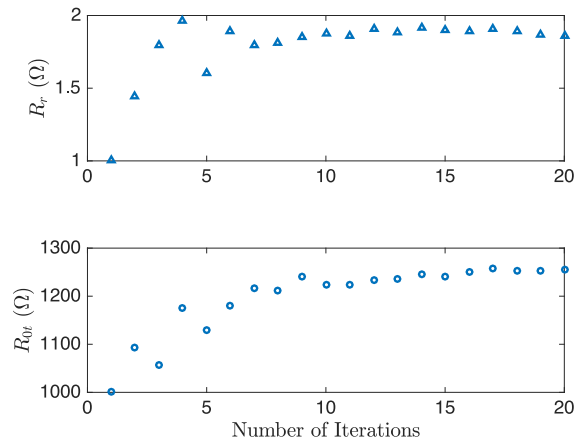
FIGURE 9. Convergence of the estimated parameters R_r and R_{0t} with approach 1 (experiment).
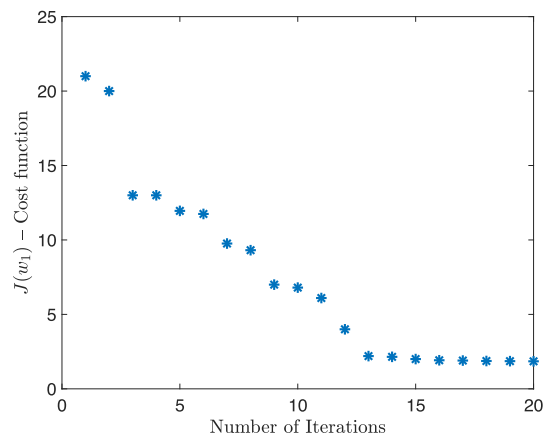
FIGURE 10. Cost function with approach 1 (experiment).
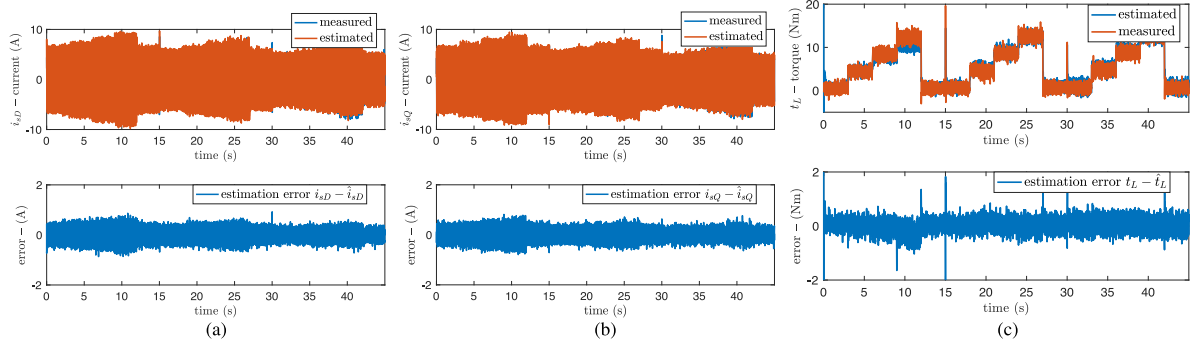
FIGURE 11. (a) Estimated and measured i_{sD} current and relative estimation error, (b) estimated and measured i_{sQ} current and relative estimation error, (c) estimated and measured load torque and relative estimation error, with parameters estimates as in approach 1 (experiments).
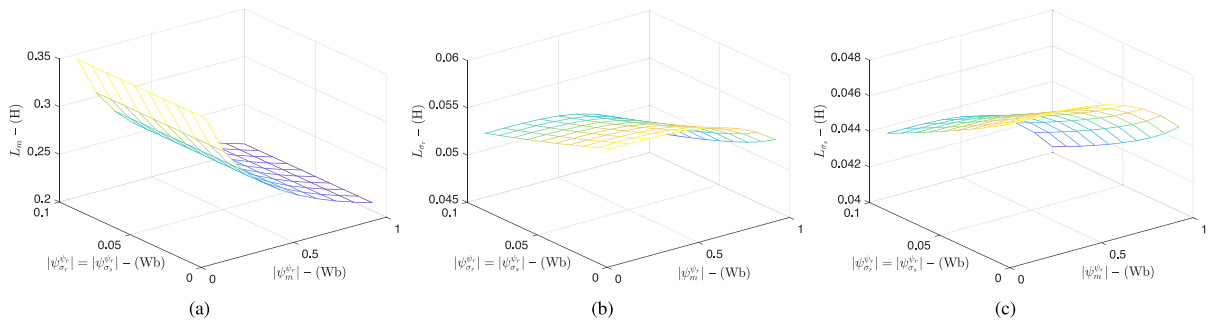
FIGURE 12. Inductances L_m in (a), L_{σ_r} in (b) and L_{σ_s} in (c) computed as in Eq.s (13) using parameters given in (28) and for different values of $|\psi_m^{\psi_r}|$ and $|\psi_{\sigma_r}^{\psi_r}| = |\psi_{\sigma_s}^{\psi_r}|$.

that the two current spikes in Fig. 5 are in correspondence of the speed variations, at 15 s and 30 s. Therefore the spikes on i_{sy} are directly related with these variation, since a speed variation implies a torque variation, which in turn implies a i_{sy} variation. The same consideration holds for the spikes on i_{sx} because a speed variation implies also a rotor flux variation. Indeed such test has been performed at variable flux corresponding to the maximum RIM efficiency for each speed/load.

In the following the results of the full identification, i.e. the results of step 2 considering the full parameters' vector, are shown. In particular as for the approach 1 related to the magnetic model of the RIM, Fig. 6–9 show the corresponding convergence curves of the estimated parameters versus the number of iterations of the algorithm, respectively L_{mu}, $L_{\sigma_s u}$, $L_{\sigma_r u}$ in Fig. 6, α_1, β_1, δ_1 in Fig. 7, a_1, b_1, c_1, d_1, in Fig. 8, and R_r, R_{0t} in Fig. 9. Fig. 10 shows the cost function versus the number of iterations. It can be easily observed that all the parameters of the model converge to their final values, corresponding to the minimum of the cost function, after more or less 10 iterations of the algorithm. Coherently, the cost function, computed considering both tests, always decreases, highlighting the goodness of the estimation process. The optimal values of vector (18) obtained after the identification process are:

$$\boldsymbol{w}_1^\star = [0.285,\ 0.048,\ 0.057,\ 1.862,\ 1256,\ 0.962,$$
$$0.876,\ 0.0738,\ 0.76,\ 0.94,\ 1.834,\ 0.166], \quad (28)$$
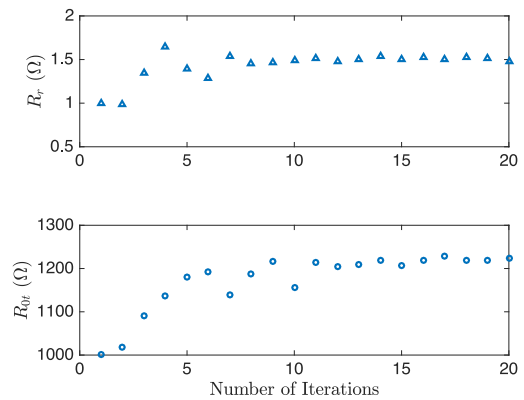

FIGURE 13. Convergence of the estimated parameters R_r and R_{0t} with approach 2 (experiment).

and the corresponding value of the cost function is: $J(\boldsymbol{w}_1^\star) = 2.021$. Moreover, it is useful to provide the computational time. In particular, using a laptop with an i5 Intel processor and a 8 Gb DDR4 RAM 1333 MHz, the time necessary, for each iteration, is about 20 seconds both for step 1 and for step 2.

Fig. 11 shows the estimated and measured current components i_{sD} and i_{sQ} and their relative estimation errors, and the estimated and measured load torque and its relative estimation error, with parameters corresponding to (28). It can be observed that estimated currents are well superimposed to the
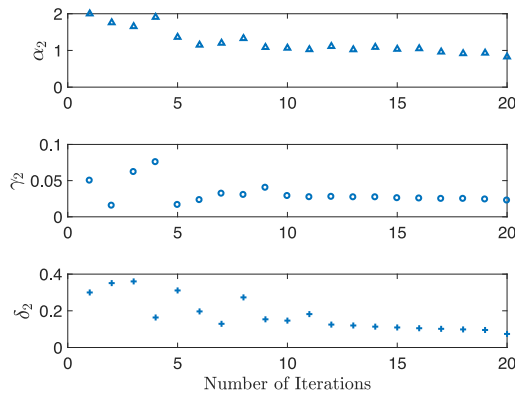
FIGURE 14. Convergence of the estimated parameters α_2, γ_2 and δ_2 with approach 2 (experiment).

FIGURE 15. Convergence of the estimated parameters β_2 and ϵ_2 with approach 2 (experiment).
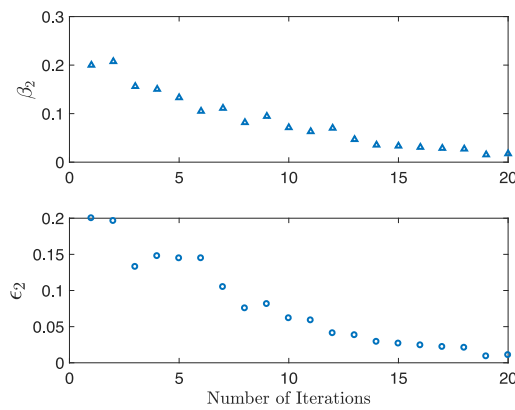

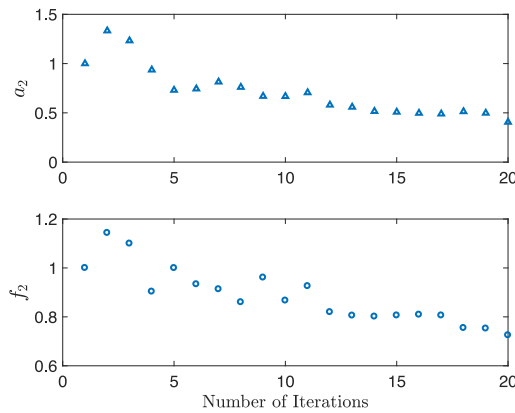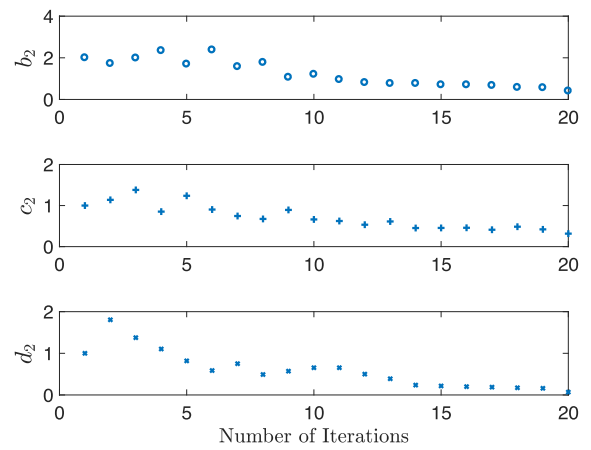**FIGURE 16.** Convergence of the estimated parameters a_2 and f_2 with approach 2 (experiment).

FIGURE 17. Convergence of the estimated parameters b_2, c_2 and d_2 with approach 2 (experiment).
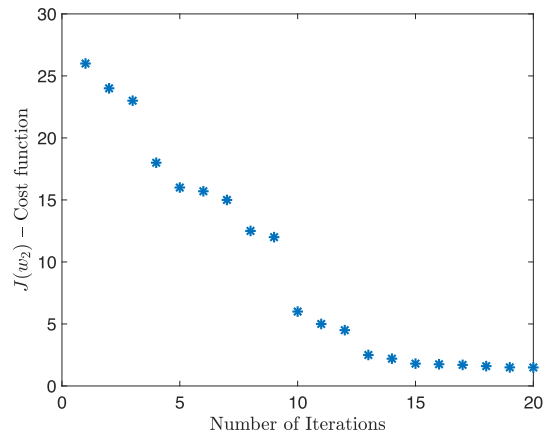

FIGURE 18. Cost function with approach 2 (experiment).

in the intervals of strong current variation (i.e. when the current crosses the zero if a sinusoidal waveform is considered). Same considerations could be made for the load torque estimation, which in average presents null estimation error and peak estimation error not exceeding 6% at the maximum load.

Finally, Fig. 12 shows the surfaces L_m, L_{σ_r} and L_{σ_s} versus $|\boldsymbol{\psi}_m^{\psi_r}|$ and $|\boldsymbol{\psi}_{\sigma_r}^{\psi_r}|$ (assuming $|\boldsymbol{\psi}_{\sigma_s}^{\psi_r}| = |\boldsymbol{\psi}_{\sigma_r}^{\psi_r}|$) computed on the basis of Eq.s (13) using parameters given in (28) at the end of the identification process. It can be observed that the three-phase magnetizing inductance reduces significantly with the magnetizing flux and less with the rotor (stator) leakage flux.

As for the approach 2 related to the magnetic model of the RIM, Fig. 13–17 show the corresponding convergence curves of the estimated parameters versus the number of iteration of the algorithm, respectively R_r, R_{0t} in Fig. 13, α_2, γ_2, δ_2 in Fig. 14, β_2, ϵ_2 in Fig. 15, a_2, f_2 in Fig. 16 and b_2, c_2, d_2 in Fig. 17. Fig. 18 shows the cost function versus the number of iterations. Even in this case, the parameters of the model converge to their final values, corresponding to the minimum of the cost function, after more or less 10 iterations of the algorithm. Coherently, the cost function, computed considering both tests, always decreases, highlighting the goodness
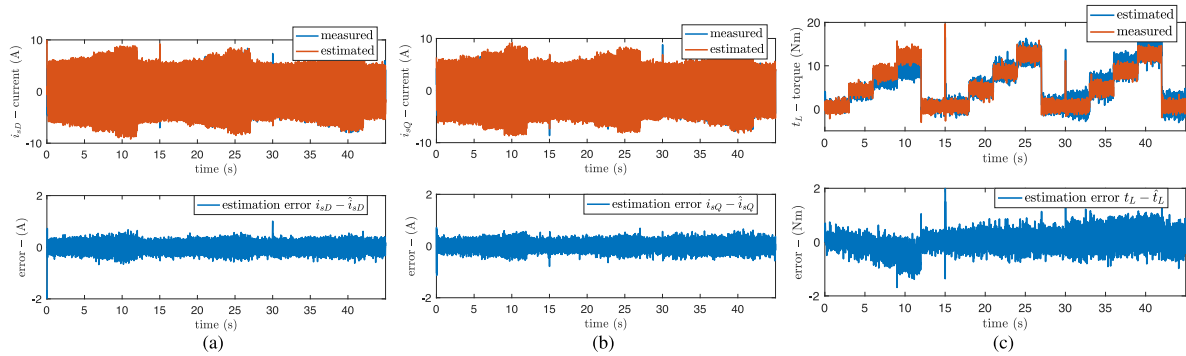
measured ones, with null average estimation error and peak estimation errors not exceeding 7%. This errors between measured and estimated quantities are mainly due to two factors: the first is the measurement noise during the experimental acquisition, and the second is a small delay that, inevitably, there is between the measured and estimated currents. Indeed, even if the two current waveforms are the same, a small delay leads to a relevant error when the difference is computed, especially

FIGURE 19. (a) Estimated and measured i_{sD} current and relative estimation error, (b) estimated and measured i_{sD} current and relative estimation error, (c) estimated and measured load torque and relative estimation error, with parameters estimates as in approach 2 (experiments).
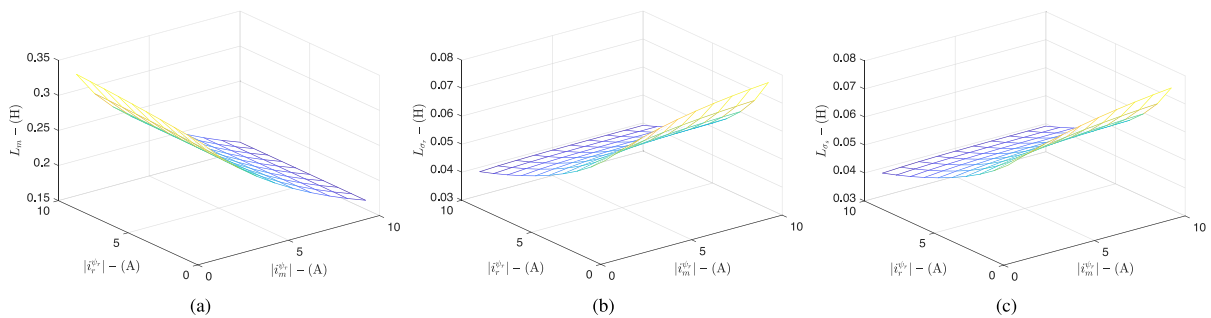

FIGURE 20. Inductances L_m in (a), L_{σ_r} in (b) and L_{σ_s} in (c) computed as in Eq.s (17) using parameters given in (29) and for different values of $|i_m^{\psi_r}|$ and $|i_r^{\psi_r}|$, and assuming the stator current equal to the sum between the magnetizing current and the rotor one.

of the estimation process. As for the parameters R_r, R_{0t}, that are estimated whatever is the approach for the description of the magnetic behavior of the RIM, their estimated values are more or less equal, with a slight difference in the estimation of R_r. The optimal values of vector (19) obtained after the identification process are:

$$w_2^\star = [1.483, \ 1223, \ 0.827, \ 0.0175, \ 0.02253, \ 0.084,$$
$$0.0107, \ 0.406, \ 0.404, \ 0.316, \ 0.0681, \ 0.725], \quad (29)$$

and the corresponding value of the cost function is: $J(w_2^\star) = 1.492$. Finally Fig. 19 shows the estimated and measured current components i_{sD} and i_{sQ} and their relative estimation errors, and the estimated and measured load torque and its relative estimation error, with parameters equal to (29). It can be observed that estimated currents are very well superimposed to the measured ones, with null average estimation error and peak estimation errors not exceeding 3%. Same considerations could be made for the load torque estimation, which in average presents null estimation error and peak estimation error not exceeding 3% at the maximum load.

Finally, Fig. 20 shows the surfaces L_m, L_{σ_r} and L_{σ_s} versus the magnetizing current and the rotor current (assuming the stator current equal to the sum between the magnetizing current and the rotor one). computed on the basis of Eq.s (17) using parameters given in (29) at the end of the identification process. It can be noted that the three-phase magnetizing inductance reduces significantly with the magnetizing current
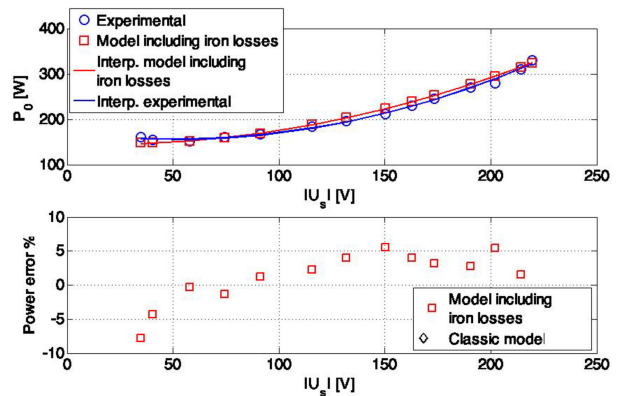

FIGURE 21. Steady-state input active power and active power error absorbed by the RIM during the no-load test (experiment).

while presenting a limited variation with the rotor current only for very low values of the magnetizing current. The rotor leakage inductance decreases mainly with the rotor current while presenting a slight increase with the magnetizing current only for very low values of the rotor current. The stator leakage inductance surface show the same shape as the rotor one, as expected.

A last experimental test has been performed in order to show the accuracy of the adopted space-vector dynamic model in predicting the iron losses. In particular Fig. 21 shows the

input active power absorbed by the RIM, and the active power percent error, versus the supply voltage amplitude at the constant supply frequency of 50 Hz (grid frequency), at no-load. In such conditions, besides the mechanical losses, which can be easily estimated on the basis of the standard no load test (as the values of the active power losses for null value of the voltage amplitude), the RIM absorbs an active power almost equal to the iron losses. The curve shows not only the measurement points, but also the second-order polynomial curve interpolating them at the best. As a matter of fact, the curve representing the behaviour of the model including the iron losses (red) is very well superimposed to the experimental curve (blue) than the corresponding curve obtained with the classic RIM model (black). Such result is confirmed by the analysis of the percent error curve that rarely exceeds 5%. Such results confirm the accuracy of the proposed model in predicting the iron losses.

VII. CONCLUSION

This paper, starting from recent papers in the scientific literature dealing with parameter estimation of RIMs, proposes a methodology for the identification of the RIM model space-vector dynamic model including both the magnetic saturation and iron losses. To this aim, the magnetic saturation effect of RIMs has been here modeled with two different approaches, respectively the first one based on current versus flux functions (approach 1) and the second one based on flux versus current functions (approach 2). Afterwards, this paper proposes an off-line technique for the estimation of electrical parameters of this model, which is based on genetic algorithms (GA). The proposed method is based on input-output measurements and needs neither the machine design geometrical data nor a FEA of the machine. It focuses on the application of an algorithm based on the minimization of a suitable cost function depending on the stator current error. The proposed electrical parameters estimation method has been initially tested in numerical simulation and further verified experimentally on a suitably developed test set-up.

REFERENCES

[1] A. Accetta, F. Alonge, M. Cirrincione, F. D'Ippolito, M. Pucci, and A. Sferlazza, "GA-based off-line parameter estimation of the induction motor model including magnetic saturation and iron losses," in *Proc. Energy Convers. Congr. Expo.*, 2017, pp. 2420–2426.

[2] H. A. Toliyat, E. Levi, and M. Raina, "A review of RFO induction motor parameter estimation techniques," *IEEE Trans. Energy Convers.*, vol. 18, no. 2, pp. 271–283, Jun. 2003.

[3] H. Tajima, G. Guidi, and H. Umida, "Consideration about problems and solutions of speed estimation method and parameter tuning for speed sensorless vector control of induction motor drives," in *Proc. Ind. Appl. Conf.*, vol. 3, 2000, pp. 1787–1793.

[4] E. Levi and M. Wang, "Online identification of the mutual inductance for vector controlled induction motor drives," *IEEE Trans. Energy Convers.*, vol. 18, no. 2, pp. 299–305, Jun. 2003.

[5] G. Kenné, R. S. Simo, F. Lamnabhi-Lagarrigue, A. Arzandé, and J. C. Vannier, "An online simplified rotor resistance estimator for induction motors," *IEEE Trans. Control Syst. Technol.*, vol. 18, no. 5, pp. 1188–1194, Sep. 2009.

[6] F. Alonge and F. D'Ippolito, "Robustness analysis of an extended Kalman filter for sensorless control of induction motors," in *Proc. Int. Symp. Ind. Electron.*, 2010, pp. 3257–3263.

[7] A. B. Proca and A. Keyhani, "Sliding-mode flux observer with online rotor parameter estimation for induction motors," *IEEE Trans. Ind. Electron.*, vol. 54, no. 2, pp. 716–723, Apr. 2007.

[8] G. R. Slemon, "Modelling of induction machines for electric drives," *IEEE Trans. Ind. Appl.*, vol. 25, no. 6, pp. 1126–1131, Nov./Dec. 1989.

[9] C. R. Sullivan and S. R. Sanders, "Models for induction machines with magnetic saturation of the main flux path," in *Proc. Ind. Appl. Soc. Annu. Meet.*, 1992, pp. 123–131.

[10] E. Levi, "A unified approach to main flux saturation modelling in DQ axis models of induction machines," *IEEE Trans. Energy Convers.*, vol. 10, no. 3, pp. 455–461, Sep. 1995.

[11] E. Levi, "Impact of cross-saturation on accuracy of saturated induction machine models," *IEEE Trans. Energy Convers.*, vol. 12, no. 3, pp. 211–216, Sep. 1997.

[12] M. Hinkkanen, A.-K. Repo, M. Cederholm, and J. Luomi, "Small-signal modelling of saturated induction machines with closed or skewed rotor slots," in *Proc. Ind. Appl. Annu. Meeting*, 2007, pp. 1200–1206.

[13] T. Tuovinen, M. Hinkkanen, and J. Luomi, "Modeling of mutual saturation in induction machines," in *Proc. Ind. Appl. Soc. Annu. Meeting*, 2008, pp. 1–8.

[14] M. Ranta, M. Hinkkanen, E. Dlala, A.-K. Repo, and J. Luomi, "Inclusion of hysteresis and eddy current losses in dynamic induction machine models," in *Proc. Int. Electr. Mach. Drives Conf.*, 2009, pp. 1387–1392.

[15] T. Tuovinen, M. Hinkkanen, and J. Luomi, "Modeling of saturation due to main and leakage flux interaction in induction machines," *IEEE Trans. Ind. Appl.*, vol. 46, no. 3, pp. 937–945, 2010.

[16] M. Ranta, M. Hinkkanen, A. Belahcen, and J. Luomi, "Inclusion of hysteresis and eddy current losses in nonlinear time-domain inductance models," in *Proc. Conf. IEEE Ind. Electron. Soc.*, 2011, pp. 1897–1902.

[17] M. Ranta and M. Hinkkanen, "Online identification of parameters defining the saturation characteristics of induction machines," *IEEE Trans. Ind. Appl.*, vol. 49, no. 5, pp. 2136–2145, Sep./Oct. 2013.

[18] M. Ranta, M. Hinkkanen, and J. Luomi, "Inductance identification of an induction machine taking load-dependent saturation into account," in *Proc. Int. Conf. Elect. Mach.*, 2008, pp. 1–6.

[19] R. Cheng, *Genetic Algorithms Eng. Optim.*. Wiley-Interscience, 2000.

[20] M. Cirrincione, M. Pucci, G. Cirrincione, and G.-A. Capolino, "A new experimental application of least-squares techniques for the estimation of the induction motor parameters," *IEEE Trans. Ind. Appl.*, vol. 39, no. 5, pp. 1247–1256, Sep./Oct. 2003.

[21] P. Vas, *Sensorless Vector Direct Torque Control*, London, U.K: Oxford Univ. Press, U.K., 1998.

[22] A. Accetta, F. Alonge, M. Cirrincione, M. Pucci, and A. Sferlazza, "Feedback linearizing control of induction motor considering magnetic saturation effects," *IEEE Trans. Ind. Appl.*, vol. 52, no. 6, pp. 4843–4854, Nov.-Dec. 2016.

[23] F. Alonge, M. Cirrincione, M. Pucci, and A. Sferlazza, "A nonlinear observer for rotor flux estimation of induction motor considering the estimated magnetization characteristic," *IEEE Trans. Ind. Appl.*, vol. 53, no. 6, pp. 5952–5965, Nov./Dec. 2017.

[24] M. Cirrincione, M. Pucci, G. Cirrincione, and G.-A. Capolino, "Constrained minimization for parameter estimation of induction motors in saturated and unsaturated conditions," *IEEE Trans. Ind. Electron.*, vol. 52, no. 5, pp. 1391–1402, Oct. 2005.

[25] H. K. Khalil, *Nonlinear Systems*, Englewood Cliffs, NJ, USA: Prentice-Hall (Inc.), 1996.

[26] M. C. Di Piazza, M. Luna, and M. Pucci, "Electrical loss minimization technique for wind generators based on a comprehensive dynamic modeling of induction machines," *IEEE Trans. Ind. Appl.*, vol. 53, no. 4, pp. 3696–3706, Jul./Aug. 2017.